Iraqi Journal of Physics, 2024 *Vol. 22, No. 4, pp.53-66*
https://doi.org/10.30723/ijp.v22i4.1244
P-ISSN: 2070-4003
E-ISSN: 2664-5548

Study of Some Structural and Optical Properties for Synthesized Graphene/Polyaniline/ZnS Nanocomposite

Elaf Kareem Salman[1a*] and Ghaida Salman Muhammed[1b]
[1]*Department of Physics, College of Science, University of Baghdad, Baghdad, Iraq*
[b*]*Corresponding Email: ghaida.muhammed@sc.uobaghdad.edu.iq*

Abstract

Hybrid graphene (GR)/ polyaniline (PANI) based composites incorporating zinc sulfide (ZnS) nanoparticles were synthesized using the drop-casting method. The weight percentage of ZnS was varied from 0.01 to 0.05%. The optical, structural, and morphological characteristics of the nanocomposite were examined utilizing X-ray diffraction (XRD), Scanning Electron Microscopy (SEM), Atomic Force Microscopic (AFM), and UV-Vis spectroscopy. The qualities and dimensions of the GR, PANI, and ZnS NPs and nanoparticle morphology resulting from the nanocomposite process were examined. Utilizing energy dispersive energy X-ray dispersive (EDX), the weight percentage of each element can be verified. The widening sharp peaks in the XRD patterns suggested the creation of a nanocrystalline phase of ZnS with a crystallite size of less than 50 nm. SEM demonstrated the interaction between ZnS nanoparticles and graphene/polyaniline. Surface topography examination using AFM shows that ZnS NPs may be effectively dispersed on top of GR/PANI structures. The ultraviolet-visible absorption spectrum (UV-Vis) showed a small absorption peak at the wavelength of 459.34nm and a broad absorption peak at 652nm.

Article Info.

Keywords:
Graphene, PANI, Zinc Sulfide, Nanocomposite, UV-VIS.

Article history:
Received: Feb. 19, 2024
Revised: Aug. 01, 2024
Accepted: Oct. 13, 2024
Published:Dec.01,2024

1. Introduction

Nanotechnology focuses on the development of materials, technologies, or structures that have a size between 1 and 100 nanometers in at least one dimension. Nanosensors represent one of the initial implementations of nanotechnology. Nanosensors refer to chemical or biological sensors that transmit information using nanomaterials [1, 2]. A chemical nanosensor is an electrical device that functions based on the physical and chemical characteristics of the nanoscale [3]. High selectivity and sensitivity, fast reaction and recovery times, low operating temperature and temperature independence, and overall stability in performance are often important requirements for effective and economical gas detection systems [4, 5]. Nanocomposites have emerged as a transformative technology that enhances the performance of chemical gas sensors. By integrating different materials at the nanoscale, these composites leverage unique properties such as increased surface area, improved conductivity, and enhanced catalytic activity, which collectively contribute to superior gas sensing capabilities. Among the many chemical gas sensors uses are in environmental monitoring, flammable gas detection, space travel, medical diagnostics, public safety, industrial pollution management, and food quality control [6].

Conducting polymers are popular chemical sensor-sensing elements due to their strong electrical and visual sensitivity to diverse gases and liquids. These polymers are easy to synthesize and sensitive at room temperature, making the sensor benefit. Because of this benefit, ammonia sensors used in industrial processes, fertilizers, food technology, clinical farms, and environmental pollution monitoring [7]. Polyaniline (PANI) is a popular conducting polymer due to its unique electrical characteristics, environmental stability, facile production, and intrinsic redox reaction [8-10]. LEDs, rechargeable batteries, and solar cells have utilized polyaniline [11-13].

PANI is a gas-sensitive conducting polymer sensitive to NH_3, CO, SO_2, and other greenhouse gases, depending on processing methods. Many researchers have made PANI-based sensors using nano-manufacturing methods and tested their quality and stability. Environmental friendliness, stability, simple synthesis, simple doping-dedoping chemistry, and low cost are some benefits of PANI [14-16].

Researchers have extensively studied transitional metal oxide nanoparticles, a significant group of inorganic nanomaterials, due to their intriguing catalytic, magnetic, and electronic properties compared to their larger counterparts. They also offer a wide range of potential applications compared to bulk materials [17, 18]. The uniform distribution of graphene oxide (GO) within the polymer matrix at the molecular level can also improve the mechanical properties, electrical conductivity, and thermal stability of the nanocomposites [19-21].

The use of the Surface Plasmon Resonance (SPR) approach is becoming increasingly popular among scientists studying various analytical techniques for tracking dangerous compounds [22, 23]. To stimulate surface plasmon, researchers typically employ a prism coupler and a gold layer. To enhance the sensitivity of SPR, researchers have built different active layers on the gold film [24-27].

Zinc sulfide (ZnS) is a versatile material with significant potential in various applications, particularly in enhancing the properties of composites. ZnS is primarily recognized for its excellent electronic and optoelectronic properties, which make it a valuable component in semiconductor applications [4].

The synthesis and characterization of ZnS nanostructures, including their crystal and morphological properties, have been extensively studied, highlighting their potential in optical devices and as green semiconductor materials. The ability to alter ZnS properties through doping and alloying further enhances its applicability in photonics, where its nonlinear optical properties are particularly beneficial [18].

ZnS is widely studied for its ability to enhance the properties of composite materials, including mechanical strength, optical characteristics, and thermal stability. As a nanofiller, ZnS improves the mechanical properties of composites like polystyrene and unsaturated polyester resin by increasing their Young's modulus and tensile strength. ZnS's nonlinear optical properties make it ideal for photonic applications, where its particle size can be controlled to tune optical absorption. Additionally, ZnS, when combined with reduced graphene oxide, significantly improves wear resistance in polyimide films. These enhancements are due to ZnS's effective interaction with the composite matrix, making it a versatile and valuable component in advanced material applications [28].

In conclusion, while the specific role of ZnS in composites is not extensively covered in the provided contexts, the material's properties and applications in related fields suggest significant potential. Future research should focus on the direct incorporation of ZnS into various composite systems to fully understand its effects and optimize its use.

This work examines the impact of different concentrations of ZnS nanoparticles on the optical, morphological, and characteristic properties of the GR/PANI polymer. The hybrid materials were analysed to evaluate their structural, optical, and morphological properties. The objective was to investigate the impact of incorporating inorganic nanoparticle additives and to assess the potential of these hybrids for developing functional materials for nanoelectronic devices. These materials offer the dual advantage of being suitable for room-temperature applications. It made a big difference in the optical properties of these hybrid nanocomposites when ZnS was added to GR/PANI.

2. Materials and Methods

2.1. Synthesis of GR/PANI, ZnS Nanoparticles

The nanocomposite was synthesized by dissolving 3 ml of graphene and 7 ml of polyaniline in 50 ml of Dimethylformamide (DMF) solvent. The graphene and polyaniline solutions were mixed in a 3:7 ratio. The reaction rate was influenced by the pH, which was regulated by the common ion effect. A second solution was prepared by dissolving 0.78 g of sodium sulfide powder (Na_2S) in 100 ml of distilled water. The two solutions were agitated at room temperature while argon gas was continuously passed through them until the formation of ZnS nanoparticles, as described by the chemical reaction [29]:

$$ZnCl_2 + Na_2S \rightarrow ZnS + 2NaCl \quad \textbf{(1)}$$

ZnS nanoparticles were added in different ratios (0.01, 0.03, 0.05wt%) to the GR/PANI compound. GR/PANI/ (0.01,0.03,0.05wt%) ZnS NPs were deposited on silicon and porous silicon using the photoelectrochemical etching method.

2.2. Materials and Instruments

All chemicals used to prepare the samples are possessed highest available purity, these chemicals and their supplying companies and the used instruments are:

Zinc Chloride powder ($ZnCl_2$), 99.999% (China), Sodium Sulfide, Hydrate flakes (Na_2S), 99.999% (HIMEDIA, India) for ZnSNPs preparation. Graphene nanopowder (5-8 nm), (skysprig nanomaterials Inc., USA). Ultrasonic; (ultrasonic cleaner with digital timer and heater capacity 5L. Furnace 220V, 50Hz, 415Watt stirrer and heater, digital timer/ heater (U.K). Magnetic stirrer (Germany) for agitation.

2.3. Characterization Techniques

The nanocomposite film was analyzed for its structural, optical, and surface morphological properties. X-ray diffraction (XRD) analysis was conducted utilizing a Philips XRD system, which records the intensity as a function of the Bragg angle. Employing Cu Kα radiation with a wavelength of 1.5406 Å, the apparatus was operated at a current of 30 mA and a voltage of 40 kV. The scanning angle 2θ was calibrated within the range of 10 to 80° at a rate of 4°/min. The interplane distance was determined for various crystal planes through the application of Bragg's law. An Atomic Force Microscope (AFM) (model-AA3000, Angstrom Advanced Inc., USA) was utilized to ascertain the average diameter and surface roughness of the nanoparticles. Through the utilization of atomic force microscopy, a multitude of characterizations of nanomaterial can be executed, encompassing the evaluation of the morphology and intrinsic properties of the observed nanostructures, homogeneity analysis to determine the statistical distribution of diverse nanomaterial's/structures within the sample, dispersion assessment to evaluate the capability of nanostructures to establish stable suspensions at designated concentration levels, whether in bundles or as isolated entities; and to assess purity throughout all phases of nanomaterial development (synthesis, purification, integration, etc.) to detect any amorphous residues within the nanostructures.

It is imperative to accurately quantify the proportion of each elemental species present in the sample. The chemical composition of graphene/polyaniline in conjunction with zinc sulfide nanoparticles deposited on a glass substrate was elucidated through Energy Dispersive X-ray (EDX) analysis. EDX is an essential instrument for ascertaining the elemental composition in a particular surface area where a fixed electron beam is directed. Scanning electron microscopy is applicable for achieving high-magnification imaging across a diverse array of materials, thereby facilitating the

analysis of the structural morphology of various samples. Surface topography evaluation was performed utilizing a Scanning Electron Microscope (SEM)(Inspect TM S50, manufactured by Bruker Nano Gmbh in Germany).

3. Results and Discussion

3.1. X-Ray Diffraction (XRD)

The XRD patterns of GR/PANI and GR/PANI/ZnS NPs with different ratios of ZnS NPs were studied, as shown in Fig. 1. The XRD pattern of the GR/PANI composites of polyaniline displayed peaks at 16.4°, 21.3°, and 23.6°, along with a peak for graphene at 26.5°. These findings align with existing research [30-33]; for GR/PANI/ZnS NPs nanocomposites with different weights addition ratios (0.01,0.03,0.05) of ZnS NPs, a phase appeared for ZnS NPs with a cubic structure. At the same time, the peaks of GR/PANI/ZnS NPs at (0.01) are shown in Fig. 1. When adding more ratios of ZnS NPs, the ZnS NPs peaks be more apparent. Adding high ratios of ZnS NPs activates the presence of cubic phase of ZnS NPs. Table 1 displays information on the peak positions and miller indices for the diffracted planes, as well as the full width at half maximum and crystallite size. The interplane spacing (d) was calculated using the relation [34]:

$$D_{hkl} = \frac{n\lambda}{2\sin\theta} \quad \textbf{(2)}$$

where λ is the X-ray wavelength (here λ = 1.54184 Å) and θ is the Bragg angle.

The average crystallite size was calculated from Scherer formula [35]:

$$D = \frac{0.9\lambda}{\beta\, cos\theta} \quad \textbf{(3)}$$

β represents the full-width at half-maximum. Variations in the ZnS NP ratio are shown in Table 1 together with the XRD characteristics of GR/PANI, and GR/PANI/ZnS NPs. The absence of changes in the ZnS peak with increasing concentration is likely due to a combination of factors, including limited crystallite growth, peak overlap with dominant GR peaks, low crystallinityof ZnS, nanoparticle agglomeration, and possible saturation effects within the composite material. These factors can obscure the expected increase in ZnS peak intensity, leading to the observed results in the XRD pattern.

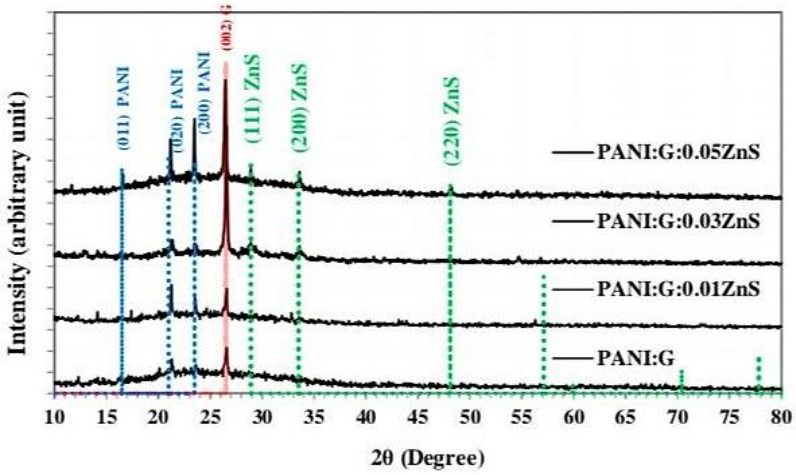

Figure 1: XRD Patterns of the GR /PANI and GR/PANI/ZnS NPs nanocomposites with different ratios of ZnS NPs.

Table 1: XRD parameters of the GR /PANI and GR/PANI/ZnS NPs composites with different ratios of ZnS NPs.

Samples	2θ (Deg.)	FWHM (Deg.)	d_{hkl} (Å)	C.S (nm)	Phase	Hkl
PANI/GR	16.402	0.462	5.3999	17.4	PANI	(011)
	21.311	0.249	4.1660	32.5	PANI	(020)
	23.623	0.285	3.7632	28.5	PANI	(200)
	26.575	0.320	3.3515	25.5	GR	(002)
PANI/GR/ 0.01 ZnS	21.240	0.213	4.1798	37.9	PANI	(020)
	23.552	0.178	3.7744	45.6	PANI	(200)
	26.575	0.213	3.3515	38.3	GR	(002)
PANI/GR/0.03 ZnS	21.347	0.285	4.1591	28.4	PANI	(020)
	23.552	0.285	3.7744	28.5	PANI	(200)
	26.540	0.213	3.3559	38.2	GR	(002)
	28.923	0.356	3.0846	23.1	Cub.ZnS	(111)
	33.618	0.462	2.6637	17.9	Cub.ZnS	(200)
PANI/GR/ 0.05 ZnS	16.616	0.178	5.3310	45.2	PANI	(011)
	21.204	0.178	4.1867	45.5	PANI	(020)
	23.516	0.178	3.7800	45.6	PANI	(200)
	26.469	0.249	3.3647	32.8	GR	(002)
	28.887	0.178	3.0883	46.1	Cub.ZnS	(111)
	33.618	0.213	2.6637	38.9	Cub.ZnS	(200)
	48.095	0.285	1.8904	30.6	Cub.ZnS	(220)

3. 2. Scanning Electron Microscopy (SEM)

For a wide range of material morphology studies, SEM is an invaluable tool. Utilizing the (Image J) software, the sizes of the nanoparticles were calculated.

SEM was used to capture high-resolution images of the nanoparticles. Fig. 2a shows an image of graphene, which has a nano sheet structure. Fig. 2b displays an image of pure ZnS NPs generated without the addition of GR/PANI. These ZnS NPs possess both a nano size and a nanoparticle structure, and they typically self-assemble. Fig. 2c shows scanning electron microscopy images of the (GR/PNAI) material revealling the presence of nanocomposites with a diameter less than 100 nm. Figures (2d, e, and f) show GR/PNAI/ZnS with different amounts of ZnS NPs. It is easy to see how the ZnS nanoparticles are attached to the GR/PANI nanosheet. The ZnS NPs successfully penetrate the GR/PANI matrix of the surrounding areas along with small composite particles [36]. The GR/PANI nanocomposite may have a relatively lower content due to an increase in ZnS NPs concentration, which could explain the diameters [37]. Table 2 show the average sizes of the GR/PNAI/ZnS nanocomposite with various ZnS NP ratios. The successful embedding of ZnS NPs into the GR/PANI nanosheets, as observed in the SEM images, suggests a strong interaction between the components, leading to the formation of stable nanocomposite. This interaction is critical for the potential applications of these materials, as it may influence their electrical, optical, and mechanical properties.

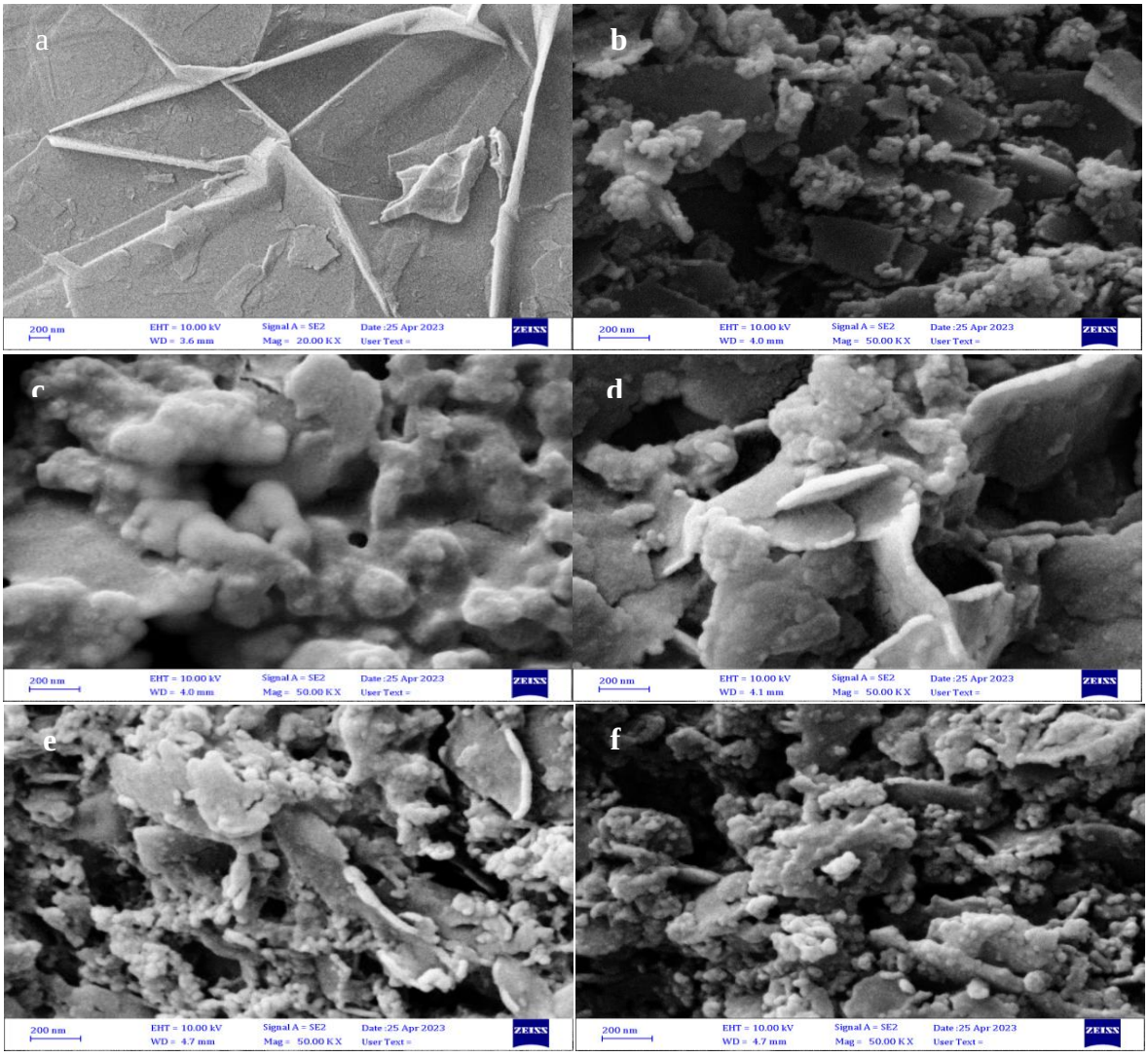

Figure 2: SEM images of (a) GR, (b) ZnS NPs, (c) GR/PANI nanocomposite, (d) GR/PANI/ZnS (0.01) nanocomposite, (e) GR/PANI/ZnS (0.03) nanocomposite and (f)GR/PANI/ZnS (0.05) nanocomposite.

Table 2: The average sizes of the GR, ZnS NPs, GR/PNAI and GR/PNAI /ZnS nanocomposite with different ratios of ZnS NPs.

Samples	Average Size (nm)
Graphene (GR)	68.081
ZnS Nanoparticles (ZnS NPs)	29.248
GR/Polyaniline (GR/PANI)	44.939
GR/PANI/ZnS NPs at 0.01	35.596
GR/PANI/ZnS NPs at 0.03	30.486
GR/PANI/ZnS NPs at 0.05	26.796

3. 2. 2. Energy Dispersive X-ray (EDX) Analysis

EDX analysis was performed, as shown in Fig. 4, to confirm the composition of the thin films components prepared. This type of analysis is necessary to know the atomic and weight ratios of the elements present in the composition of the prepared thin films. The graphs revealed the presence of carbon, oxygen, sulfate zinc which was expected. Peaks of Zn in Fig. 4d, e, and f demonstrate the presence of the semiconductor in graphene/polyaniline nanocomposite, where the compositional elements ratios measured match those predicted by the stoichiometric formula [38]. In

our EDX analysis, the presence of elements, such as Au, Si, Na, and Mo was detected, their presence is explained as follows:

- Gold **(Au):** likely due to gold coating on the samples for the electron microscopy or the presence of gold nanoparticles used during synthesis.
- Silicon **(Si):** probably from the silicon substrate on which the samples were deposited, which is common in thin-film and nanocomposite studies.
- Sodium **(Na):** could have originated from residual salts or chemicals used in the synthesis or sample preparation process.
- Molybdenum **(Mo):** possibly from the sample holder or molybdenum-containing materials used in the experimental set.

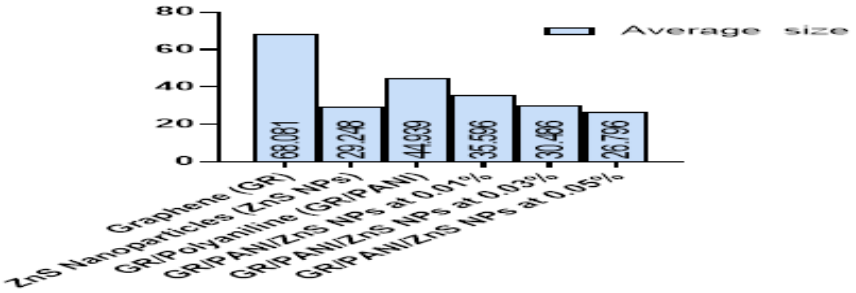

Figure 3: The average sizes of the GR, ZnS NPs, GR/PNAI and GR/PNAI /ZnS Nanocomposite with different ratios of ZnS NPs.

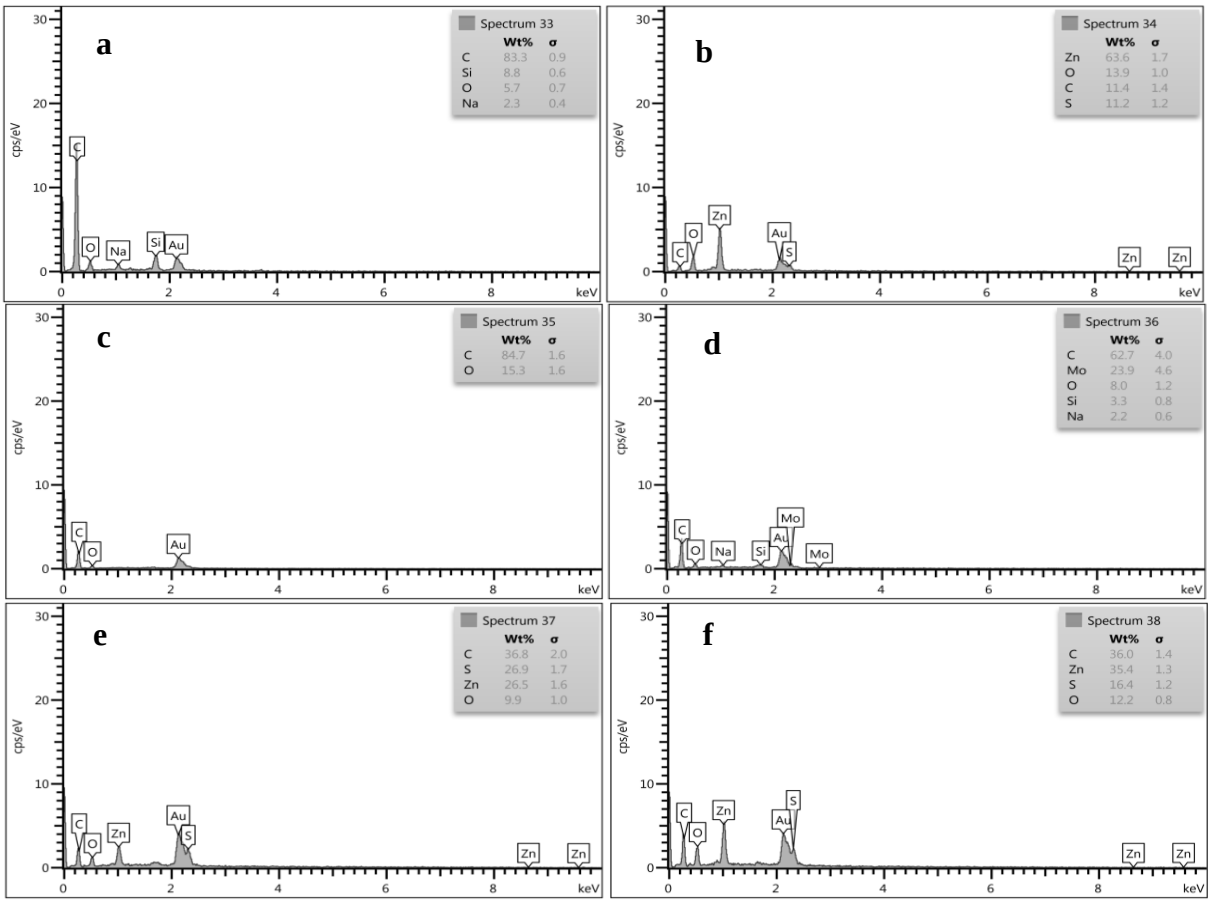

Figure 4: EDX analysis of (a) GR, (b) ZnS NPs, (c) GR/PANI nanocomposite, (d) GR/PANI/ZnS (0.01) nanocomposite, (e) GR/PANI/ZnS (0.03) nanocomposite and (f) GR/PANI/ZnS (0.05) nanocomposite.

3. 2. 3. Atomic Force Microscopy (AFM)

Atomic force microscopy (AFM) is employed to establish the thickness, surface morphology and surface roughness of the GR, GR/PANI and GR/PANI/ZnS nanocomposite with different ratios of ZnS NPs. The surface was characterized by a uniform array of nano particulate GR/PANI nodules. The images (Fig. 5) indicated homogeneous and continuous films. Roughness parameters are compared for all the three depositions in Table 3. The rippled like structure of the GR, GR/PANI and GR/PANI/ZnS nanocomposite is further confirmed by the AFM study [39]. The way ZnS nanoparticles are distributed can impact surface roughness and grain structure. More homogeneous distributions typically lead to smoother surfaces, while uneven distributions can cause roughness. Changing the ratio of ZnS to PANI affects the matrix's structure. Different ratios can lead to varying degrees of surface irregularity and changes in grain size**.**

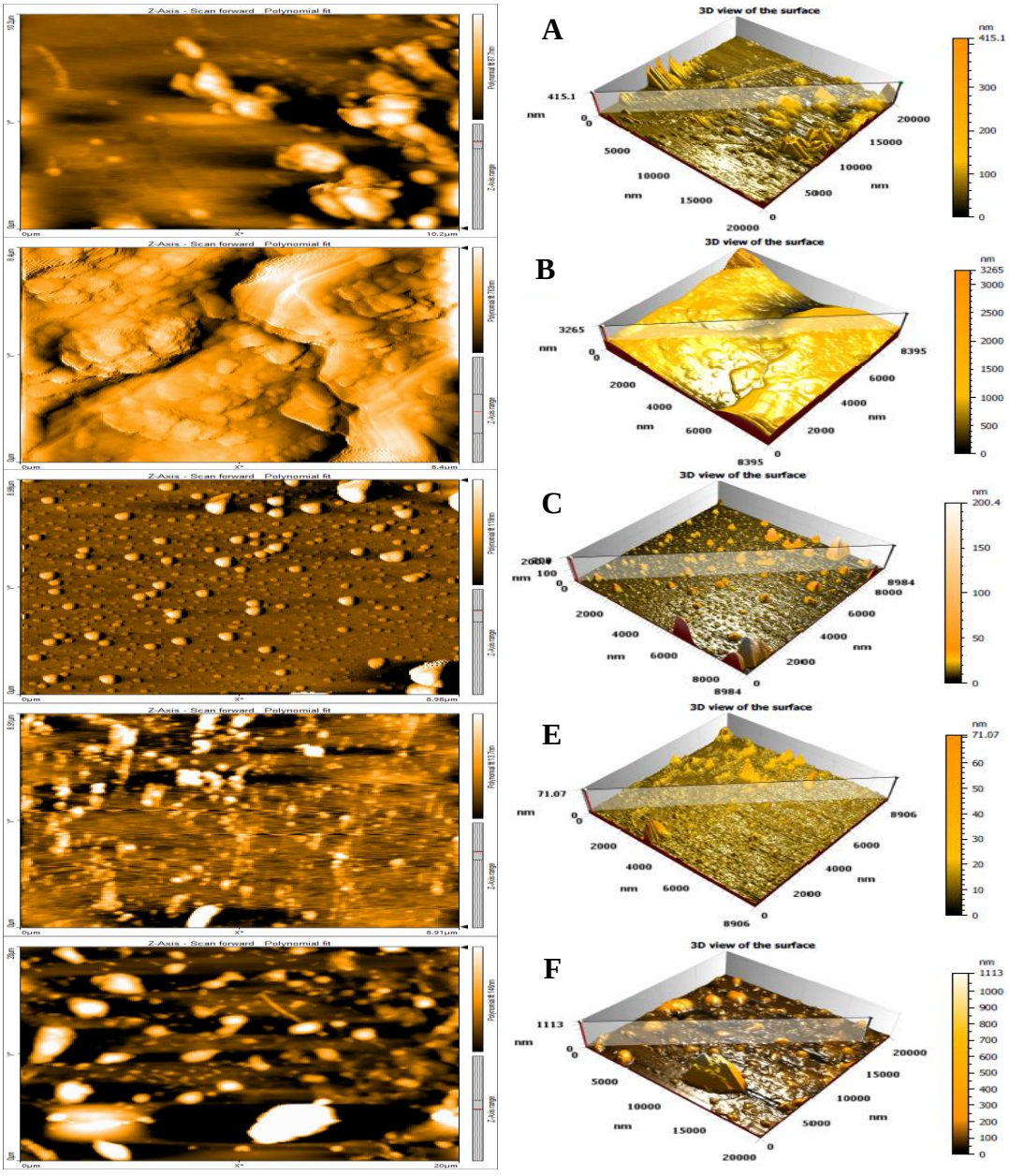

Figure 5: AFM images (2D, 3D) for surface morphology of (a) GR, (b) ZnS NPs, (c) GR/PANI nanocomposite, (d) GR/PANI/ZnS (0.01) nanocomposite, (e)GR/PANI/ZnS (0.03) nanocomposite and (f) GR/PANI/ZnS (0.05) nanocomposite.

The surface characteristics of the GR, GR/PANI, and GR/PANI/ZnS nanocomposite vary significantly with the ZnS NP ratio. Lower ZnS concentrations (0.01) increased surface roughness, while intermediate concentrations (0.03) provided a smoother surface. Higher ZnS concentrations (0.05) increased the roughness again, likely due to nanoparticle agglomeration. These findings shows the importance of optimizing ZnS NP ratios to achieve the desired surface properties for specific applications.

Table 3: Values of surface roughness, mean roughness square (RMS) and grain size of GR, GR/PNAI and GR/PNAI /ZnS nanocomposite with different ratios of ZnS NPs.

Samples	**Sa (nm)**	**Sq (nm)**	**Sz (nm)**	**Ave.G.S.(nm)**
GR	25.19	36.78	415.4	258
GR/PANI	204.7	255.1	1560	94.57
GR/PANI/ ZnS NP_s at (0.01)	67.33	263.6	3798	73.76
GR/PANI/ ZnS NP_s at (0.03)	2.867	4.576	69.09	74.08
GR/PANI/ ZnS NP_s at (0.05)	55.92	104.9	1142	104.5

3.3. UV-Vis Absorption Spectra

UV–Vis spectra for ZnS, GR/PANI and GR\PANI\ZnS NPs nanocomposite of (0.01,0.03,0.05wt%) are shown in Fig. 6. The spectra show a small absorption peak at 459.34 nm and a wide absorption peak at 652 nm. The π–π* transition causes a 459.34 nm absorption band, while the quinoid ring transition causes a 652 nm absorption band in polyaniline chains. Similar results were found by Fauzi et al. [40].

The ratio of the incident light's intensity, absorption, and transmission (I_T/I) provides the formula for the film's transmittance, denoted as T [41]:

$$T = \frac{I_T}{I} \qquad (4)$$

where: T is the transmittance,I_T is the transmitted light intensity,and I is the light intensity.

The absorbance of the sample is defined as the negative log of the transmittance given by the relation [42]:

$$A = -\log_{10} T \qquad (5)$$

where: A is the absorbance of the sample.

When ZnS nanoparticles were added to GR and PANI in the GR/PANI/ZnS nanocomposite, the ZnS nanoparticles' wavelength increased. When tiny particles aggregate and consolidate, the bands amplify a more complicated growth mechanism [43, 44]. This finding is consistent with previous findings reported by Fauzi et al. [40] .

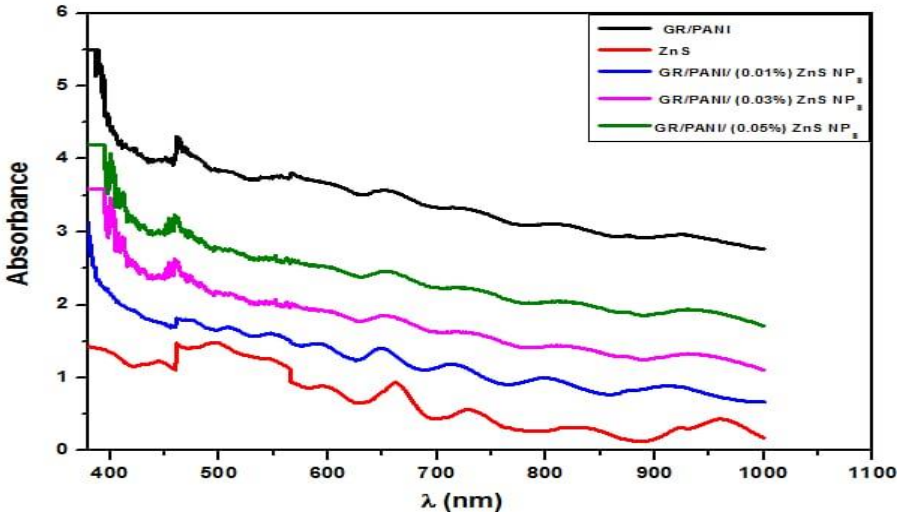

Figure 6: UV–Vis absorption spectra of the ZnS, GR/PNAI and GR/PNAI /ZnS Nanocomposite with different ratios of ZnS NPs.

SPR is a sophisticated optical phenomenon that occurs at the interface between a metal and a dielectric material. It involves the resonant oscillation of conduction electrons stimulated by incident light, resulting in a surface wave known as a surface Plasmon. Table 4 illustrates the SPR values of various materials, including composites of GR, PANI, and ZnS nanoparticles. These values indicate the specific wavelengths at which electron oscillations occur on the material's surface. The GR/PANI material and ZnS both exhibited an SPR value of 461 nm, while the composite materials with varying ratios of ZnS nanoparticles showed slight variations in their SPR values, ranging from 459 nm to 463 nm. These variations shows how the material's surface properties change with different amounts of zinc sulfide [45], as seen in Table 4. When ZnS nanoparticles were incorporated into the GR/PANI matrix, the absorption spectra of the composite materials exhibited shifts in their absorption peaks. Specifically, the introduction of ZnS nanoparticles can lead to a shift in the wavelength of maximum absorption due to changes in the electronic structure and interaction between the nanoparticles and the surrounding matrix. This shift in absorption wavelength can be attributed to several factors, which are:

SPR: The presence of ZnS nanoparticles may induce changes in the SPR characteristics of the composite. This can result in a shift of the absorption peaks to longer or shorter wavelengths depending on the size, shape, and concentration of the nanoparticles.

Particle size and aggregation: The size and aggregation state of ZnS nanoparticles can affect their optical properties. Aggregation or changes in nanoparticle size can cause variations in the absorption wavelength and the intensity of absorption peaks.

Interaction with the matrix: ZnS nanoparticles interact with the GR/PANI matrix, altering the electronic environment and thereby influencing the absorption spectrum. This interaction can lead to a shift in the absorption peaks, reflecting changes in the electronic transitions within the composite material.

In summary, ZnS nanoparticles' wavelength increase refers to the observed shift in the absorption peak of the composite material due to the incorporation of ZnS nanoparticles, which affects the optical properties and absorption behavior of the material.

The energy band gap values for graphene/polyaniline were found to be 2.06 eV, while for zinc sulfide, it was determined to be 1.88 eV. It has been noted, as shown in Fig. 7, that after the incorporation of ZnS in varying proportions (0.01,0.03,0.05wt%) into GR/PANI, the optical energy gap decreased from 2.06 eV to 1.89 eV, subsequently

to 1.5 eV, and finally to 1.4 eV. This reduction can be attributed to the chemical interactions between graphene and the ZnS nanoparticles. Such a variation underscores that the integration of graphene significantly alters the electronic characteristics of ZnS nanoparticles, thus enhancing the electrical conductivity of the composite material [46].

Table 4: Surface Plasmon Resonance (SPR) of GR/PANI, Zn and GR/PANI /ZnS nanocomposite with different ratios of ZnS NPs

Samples	Surface Plasmon Resonance (SPR)
GR/PANI	461
ZnS	461
GR/PANI/ ZnS NP_s at (0.01)	463
GR/PANI/ ZnS NP_s at (0.03)	460
GR/PANI/ ZnS NP_s at (0.05)	459

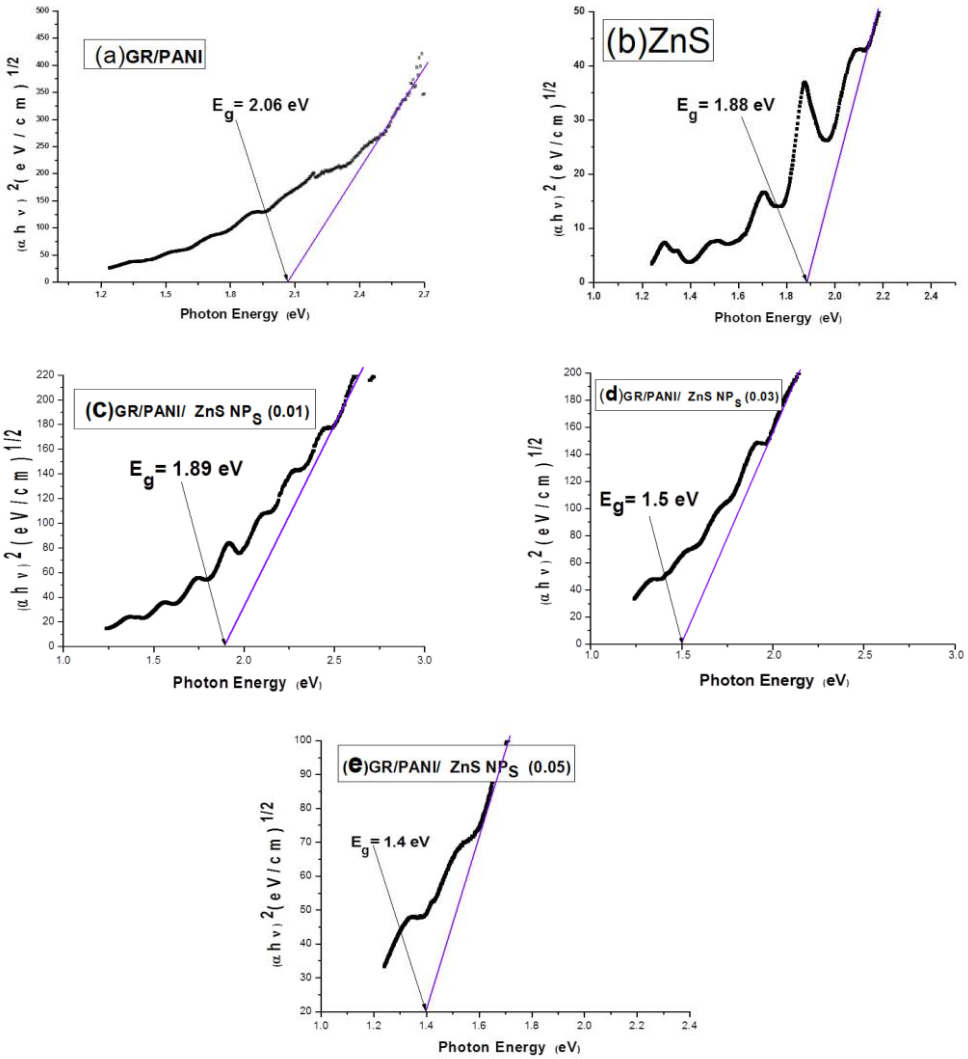

Figure 7: Energy gap of (a) GR/PANI, (b)ZnS, (C)GR/PANI/ZnS (0.01), (d) GR/PANI/ZnS (0.03), (e) GR/PANI/ZnS (0.05).

4. Conclusions

In this study, GR/PANI nanocomposite incorporating ZnS nanoparticles were successfully synthesized using drop casting method with varying ZnS weight

percentages (0.01 to 0.05). Comprehensive characterization were done through XRD, SEM, AFM, and UV-Vis spectroscopy. The structural and optical characteristics of nanocomposite might be enhanced by combining nanoparticles with GR/PANI nanocomposite. The possibility of preparing samples from GR/PANI nanocomposite and GR/PANI/ZnS NPs (0.01,0.03,0.05wt%) by drop casting method, and these prepared samples were deposited on silicon and porous silicon substrates which prepared by photoelectrochemical etching method. XRD analysis reveals that GR/PANI hexagonal structure and ZnS exhibit cubic structure. The UV-Vis spectra of the composites revealed no extra peaks as the ZnS concentration increases, this suggests that the ZnS NPs might be effectively dispersed on top of the GR/PANI structures. In conclusion, the study demonstrated that the incorporation of ZnS nanoparticles into GR/PANI composites not only enhanced the optical properties but also maintained the material's structural stability, offering significant potential for future applications in advanced material science. The incorporation of ZnS nanoparticles significantly impacts the material's characteristics, suggesting potential applications in advanced electronic and photonic devices.

Acknowledgements

The authors would like to thank the Department of Physics, College of Science, University of Baghdad for their assistance in carrying out this work.

Conflict of interest

Authors declare that they have no conflict of interest.

References

1. A. N. Naje and W. K. Mahmood, IOP Conf. Ser. Mat. Sci. Eng. **454**, 012070 (2018). DOI: 10.1088/1757-899X/454/1/012070.
2. A. Eatemadi, H. Daraee, H. Karimkhanloo, M. Kouhi, N. Zarghami, A. Akbarzadeh, M. Abasi, Y. Hanifehpour, and S. W. Joo, Nanosc. Res. Lett. **9**, 393 (2014). DOI: 10.1186/1556-276X-9-393.
3. G. Di Francia, B. Alfano, and V. La Ferrara, J. Sen. **2009**, 659275 (2009). DOI: 10.1155/2009/659275.
4. Y. Wang and J. T. W. Yeow, J. Sen. **2009**, 493904 (2009). DOI: 10.1155/2009/493904.
5. S. K. Abbas and A. N. Naje, Nano Hyb. Comp. **30**, 1 (2020). DOI: 10.4028/www.scientific.net/NHC.30.1.
6. W. K. M. a. N. N. Murad M. Kadhim, Design Eng. **2021**, 6485 (2021).
7. C. Wrenn, Occup. H. Saf. **69**, 64 (2000).
8. R. L. N. Chandrakanthi and M. A. Careem, Thin Sol. Fil. **417**, 51 (2002). DOI: 10.1016/S0040-6090(02)00600-4.
9. P. Somani, B. B. Kale, and D. P. Amalnerkar, Synth. Met. **106**, 53 (1999). DOI: 10.1016/S0379-6779(99)00109-5.
10. Y. He, Mat. Chem. Phys. **92**, 134 (2005). DOI: 10.1016/j.matchemphys.2005.01.033.
11. S.-A. Chen, K.-R. Chuang, C.-I. Chao, and H.-T. Lee, Synth. Met. **82**, 207 (1996). DOI: 10.1016/S0379-6779(96)03790-3.
12. A. G. Macdiarmid, L. S. Yang, W. S. Huang, and B. D. Humphrey, Synth. Met. **18**, 393 (1987). DOI: 10.1016/0379-6779(87)90911-8.
13. D. Verma and V. Dutta, Sen. Actuat. B Chem. **134**, 373 (2008). DOI: 10.1016/j.snb.2008.05.009.
14. N. Kumar, L. P. Purohit, and Y. C. Goswami, Phys. E Low-dimen. Syst. Nanostruct. **83**, 333 (2016). DOI: 10.1016/j.physe.2016.04.025.
15. J. Y. Shimano and A. G. Macdiarmid, Synth. Met. **123**, 251 (2001). DOI: 10.1016/S0379-6779(01)00293-4.
16. W. Lyu, M. Yu, J. Feng, and W. Yan, Appl. Surf. Sci. **458**, 413 (2018). DOI: 10.1016/j.apsusc.2018.07.074.
17. S. K. Abbas and A. N. Naje, Iraqi J. Phys. **18**, 62 (2020). DOI: 10.30723/ijp.v18i47.579.
18. R. Mohapatra, J. Kaundal, and Y. Goswami, Chalcogen. Lett. **18**, 255 (2021). DOI: 10.15251/CL.2021.185.255.

19. P. Govindaraj, A. Sokolova, N. Salim, S. Juodkazis, F. K. Fuss, B. Fox, and N. Hameed, Comp. Part B Eng. **226**, 109353 (2021). DOI: 10.1016/j.compositesb.2021.109353.
20. K. M. Abu Hurayra–Lizu, M. W. Bari, F. Gulshan, and M. R. Islam, Heliyon **7**, e06983 (2021). DOI: 10.1016/j.heliyon.2021.e06983.
21. S. Z. Al Sheheri, Z. M. Al-Amshany, Q. A. Al Sulami, N. Y. Tashkandi, M. A. Hussein, and R. M. El-Shishtawy, Desig. Monom. Poly. **22**, 8 (2019). DOI: 10.1080/15685551.2019.1565664.
22. F. B. Kamal Eddin, Y. W. Fen, N. a. S. Omar, J. Y. C. Liew, and W. M. E. M. M. Daniyal, Spectrochim. Acta Part A Molec. Biomoloc. Spect. **263**, 120202 (2021). DOI: 10.1016/j.saa.2021.120202.
23. N. a. S. Omar, Y. W. Fen, I. Ramli, A. R. Sadrolhosseini, J. Abdullah, N. A. Yusof, Y. M. Kamil, and M. A. Mahdi, Polymers **13**, 762 (2021). DOI: 10.3390/polym13050762.
24. F. B. Kamal Eddin and Y. Wing Fen, Sensors **20**, 1039 (2020). DOI: 10.3390/s20041039.
25. N. S. M. Ramdzan, Y. W. Fen, N. a. A. Anas, N. a. S. Omar, and S. Saleviter, Molecules **25**, 2548 (2020). DOI: 10.3390/molecules25112548.
26. M. D. A. Roshidi, Y. W. Fen, W. M. E. M. M. Daniyal, N. a. S. Omar, and M. Zulholinda, Optik **185**, 351 (2019). DOI: 10.1016/j.ijleo.2019.03.118.
27. F. B. Kamal Eddin and Y. W. Fen, Molecules **25**, 2769 (2020). DOI: 10.3390/molecules25122769.
28. R. Bisauriya, S. Khandelwal, and Y. C. Goswami, Mat. Today Proce. **47**, 6379 (2021). DOI: 10.1016/j.matpr.2021.08.171.
29. G. Salman, M. Medhat, and A. Muhammed, Australian J. Bas. Appl. Sci. **11**, 29 (2017).
30. F. E. Jorge, L. G. P. Tienne, and M. De Fátima Vieira Marques, Mat. Sci. Eng. B **263**, 114851 (2021). DOI: 10.1016/j.mseb.2020.114851.
31. T. N. J. I. Edison, R. Atchudan, N. Karthik, P. Chandrasekaran, S. Perumal, P. Arunachalam, P. B. Raja, M. G. Sethuraman, and Y. R. Lee, Surf. Coat. Tech. **416**, 127150 (2021). DOI: 10.1016/j.surfcoat.2021.127150.
32. Alamgeer, M. Tahir, M. R. Sarker, S. Ali, Ibraheem, S. Hussian, S. Ali, M. Imran Khan, D. N. Khan, R. Ali, and S. Mohd Said, Polymers **15**, 363 (2023). DOI: 10.3390/polym15020363.
33. A. H. Mohammed, A. N. Naje, and R. K. Ibrahim, Iraqi J. Sci. **63**, 5218 (2022). DOI: 10.24996/ijs.2022.63.12.12.
34. C. Kittel and P. Mceuen, *Introduction to Solid State Physics* (USA, John Wiley & Sons, 2018).
35. L. Kernazhitsky, V. Shymanovska, T. Gavrilko, V. Naumov, and V. Kshnyakin, Ukrainian J. Phys. Opt. **14**, 15 (2013). DOI: 10.3116/16091833/14/1/15/2013.
36. I. M. Ali, Iraqi J. Phys. **17**, 21 (2019). DOI: 10.20723/ijp.17.40.21-32
37. M. Parmar, C. Balamurugan, and D.-W. Lee, Sensors **13**, 16611 (2013). DOI: 10.3390/s131216611.
38. B. Zhou, Y.-W. Zhang, C.-S. Liao, C.-H. Yan, L.-Y. Chen, and S.-Y. Wang, J. Mag. Mag. Mat. **280**, 327 (2004). DOI: 10.1016/j.jmmm.2004.03.031.
39. F. M. Ahmed and S. M. Hassan, Iraqi J. Phys. **19**, 72 (2021). DOI: 10.30723/ijp.v19i51.652.
40. N. I. M. Fauzi, Y. W. Fen, J. Abdullah, M. A. Kamarudin, N. a. S. Omar, F. B. K. Eddin, N. S. M. Ramdzan, and W. M. E. M. M. Daniyal, Photonics **9**, 300 (2022). DOI: 10.3390/photonics9050300.
41. H. Gupta, B. L. Choudhary, S. Ahmad, K. P. Tewari, and P. A. Alvi, American Institute of Physics Conference Series (India AIP, 2020). p. 130008.
42. S. S. H. Al-Mgrs, M. H. Al-Timimi, M. Z. Abdullah, and W. H. Al-Banda, AIP Conf. Proc. **2475**, 090018 (2023). DOI: 10.1063/5.0102768.
43. A. K. M. Al-Sammarraie, J. Glob. Pharm. Tech. **11**, 419 (2019).
44. K. M. Ibrahim, W. R. Saleh, and A. M. A. Al-Sammarraie, Nano Hyb. Comp. **35**, 75 (2022). DOI: 10.4028/p-0w806z.
45. Rohit and J.-J. Huang, Conference on Lasers and Electro-Optics/Europe (CLEO/Europe 2023) and European Quantum Electronics Conference (EQEC 2023) (Munich Optica Publishing Group, 2023). p. ch_15_4.
46. R. Ramachandran, M. Saranya, P. Kollu, B. P. C. Raghupathy, S. K. Jeong, and A. N. Grace, Electrochim. Acta **178**, 647 (2015). DOI: 10.1016/j.electacta.2015.08.010.

دراسة بعض الخصائص التركيبية والضوئية لمركب الكرافين/البولي انيلين/كبريتيد الزنك النانوي المحضر

ايلاف كريم سلمان[1] و غيداء سلمان محمد[1]
[1] قسم الفيزياء، كلية العلوم، جامعة بغداد، بغداد، العراق

الخلاصة

تم تصنيع مركبات هجينة من الجرافين (GR) / البولي انيلين (PANI) تتضمن جسيمات نانوية من كبريتيد الزنك (ZnS) باستخدام الطريقة الصب النقطي وتتراوح نسبة وزن ZnS من 0.01 إلى 0.05 .تم تشخيص الخواص التركيبية والمورفولوجية والبصرية للمركب النانوي بواسطة قياسات حيود الأشعة السينية XRD والمجهر الإلكتروني الماسح (SEM)و تم تقييم صفات وأبعاد الجرافين وكبريتيد الزنك وبلورات البوليانيلين باستخدام حيود الأشعة السينية (XRD). وباستخدام المجهر الإلكتروني الماسح (SEM)و مجهر القوة الذرية (AFM)و طيف الامتصاص فوق البنفسجي المرئي (UV-VIS) ، تم فحص العيوب ومورفولوجيا الجسيمات النانوية الناتجة عن عملية التركيب النانوي. باستخدام التحليل الطيفي للأشعة السينية المشتتة من الطاقة (EDX)، يمكن التأكد من النسبة الوزنية لكل عنصر. تم اقتراح إنشاء مرحلة بلورية نانوية من ZnS بحجم بلوري أقل من 50 نانومتر من خلال القمم الحادة الظاهرة في أنماط XRD. أظهرت هذه الصور المجهر الإلكتروني الماسح التفاعل بين جسيمات ZnS النانوية والجرافين/البوليانيلين. يُظهر فحص مورفولوجيا السطح باستخدام مجهر القوة الذرية (AFM) وطرق أخرى أنه يمكن ان تنتشر ZnS NPs بشكل فعال فوق هياكل GR / PANI. اظهر طيف الامتصاص فوق البنفسجي المرئي (UV-VIS) ذروة امتصاص صغيرة عند الطول الموجي.459.39 نانومتر وقمة امتصاص واسعة عند 652 نانومتر.

الكلمات المفتاحية: الكرافين، البولي انيلين، كبريتيد الزنك، المركب النانوي، طيف الامتصاص فوق البنفسجي المرئي.